

Heterogeneous firing response of mice layer V pyramidal neurons in the *fluctuation-driven* regime

Y. ZERLAUT^{1,2}, B. TELENCZUK^{1,2}, C. DELEUZE¹, T. BAL¹, G. OUANOUNOU^{1*} & A. DESTEXHE^{1,2*}

January 13, 2016

I Abstract

Characterizing the input-output properties of neocortical neurons is of crucial importance to understand the properties emerging at the network level. In the regime of low-rate irregular firing (such as in the *awake* state) determining those properties for neocortical cells remains, however, both experimentally and theoretically challenging. Here, we identified three somatic variables that describe the dynamical state at the soma in the *fluctuation-driven* regime: the mean, standard deviation and speed of the membrane potential fluctuations. We characterized the firing rate response of individual layer V pyramidal cells in this three-dimensional space by means of *dynamic-clamp* and perforated patch recordings in the visual cortex of juvenile mice *in vitro*. We found that *single neurons* strongly differ *from each other* in terms of their excitability and sensitivities to the variations in the three parameters of the fluctuations. We show with theoretical modeling that heterogeneous levels of biophysical properties such as sodium inactivation, sharpness of sodium activation and spike frequency adaptation might be the main contributors to the observed diversity of firing responses. Because the firing rate response will determine population rate dynamics during asynchronous neocortical activity, our results show that cortical populations are functionally strongly inhomogeneous in young mice visual cortex, which should have important consequences on cortical computation at early stages of sensory processing.

II Significance statement

Heterogeneity is an ubiquitous property of biological systems, but characterizing its extent and functional impact represents a challenge for experimentalists. Here we developed a method to characterize the response of single neocortical layer V pyramidal cells of young mice visual cortex in an activity domain imitating normal awake state. We

found that individual neurons greatly differ not only in their excitability but also in their ability to trigger spikes as a function of the characteristics of the membrane potential fluctuations. By highlighting and quantifying this diversity, our study contributes to the understanding of how biological heterogeneity impacts neocortical computations.

III Introduction

The neocortex of awake animals displays an activated state in which cortical activity manifests highly complex, seemingly noisy behavior. At the level of single neurons the activity is characterized by strong subthreshold fluctuations and irregular firing at low rate: this constitutes the fluctuation-driven regime, which is believed to be central to cortical computations (Destexhe and Contreras, 2006). Since sensory processing of natural stimuli also evoke sparse response at low population rates, see for example ? in cat V1, understanding the dynamical and computational properties of this regime at the cellular and network level is a key challenge in systems neuroscience.

On the other hand sparse responses at low population rates constitute a difficulty for experimentalists *in vivo* as responses are of low amplitude and render experimental characterization challenging. To a lesser extent, this is also true *in vitro*, characterizing the spiking response of single neurons at low rate requires long recording times and stable properties. In the present paper, we propose a characterization of the low rate response of single neurons that was made possible by the combination of the stability offered by the perforated patch technique technique and a simple fitting procedure for the spiking response.

We investigate single neuron responses with respect to three somatic variables: the mean, standard deviation and speed of the membrane potential fluctuations at the soma. In comparison with previous work (La Camera et al., 2008), our approach allows to investigate the response to fast membrane potential fluctuations present in the *high conductance* state of cortical networks (Destexhe et al., 2003). This characterization focuses on how these fluctuations are translated into output spikes on top of subthreshold integration effects (Kuhn et al., 2004). In addition, we also investigated the putative biophysical origin of the measured responses in established theoretical models of single neurons.

IV Results

The paper is organized as follows: we start by defining the fluctuation-driven regime at the soma and designing a method to reproduce this somatic dynamical state under

¹ Unité de Neurosciences, Information et Complexité, Centre National de la Recherche Scientifique, FRE 3693, Gif sur Yvette, France

² European Institute fo Theoretical Neuroscience, 74 Rue du Faubourg Saint-Antoine, 75012 Paris

correspondance : destexhe@unic.cnrs-gif.fr

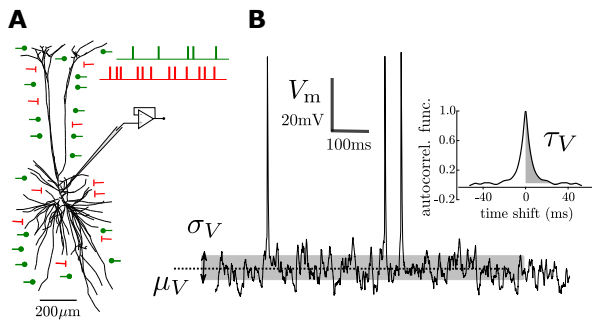


Figure 1: Investigating somatic computation in the fluctuation-driven regime **(A)** Schematic illustration on a layer V pyramidal cell in cat V1 (?) together with theoretical distribution of inhibitory (red) and excitatory (green) synaptic inputs. Synaptic and dendritic integration of pre-synaptic spike trains (two sample spike trains in upper right) produce membrane potential fluctuations at the soma as recorded intracellularly in current-clamp. **(B)** A sample trace of membrane potential integrating inputs from all inhibitory and excitatory synapses (black trace). We characterize those fluctuations by a mean μ_V (dashed horizontal line), a standard deviation σ_V of sub-threshold oscillations (gray background) and global autocorrelation time τ_V (determined from the normalized autocorrelation function in the inset, see Methods VI.6). The properties of those fluctuations determine the spiking probability of the neuron (three spikes visible in the membrane-potential trace).

dynamic-clamp experiments. We also derive a flexible template for the firing rate response, whose accuracy is demonstrated on various theoretical models. Then, we investigate the firing response of layer V pyramidal cells in mice juvenile cortex and we analyze the individual features of single neuron responses. Finally, we explore the putative biophysical origin of the observed response in theoretical models of neocortical neurons.

IV.1 A three-dimensional description of the dynamical state at the soma in the fluctuation-driven regime

Determining the cellular input-output functions is complex because input of neocortical neurons are mostly in dendrites and output spikes are generated in initial segments of an axon as reviewed in ? and Debanne et al. (2011) input will therefore crucially shape their input-output relationship. Various parameters of presynaptic activity can arbitrarily control the properties of the membrane potential fluctuations at the soma. Those properties can be quantified by identifying three somatic variables that provide a reduced description of the dynamical state at the soma in the *fluctuation-driven* regime: the mean μ_V , the standard deviation σ_V of the membrane potential fluctuations and their typical autocorrelation time τ_V (see Methods VI.6). For example, the excitatory/inhibitory balance controls the mean depolarization at the soma μ_V , the mean synaptic bombardment impacts the standard deviation σ_V and the speed of the membrane potential

fluctuations τ_V . Other effects such as synchrony in the presynaptic spike trains or ratio between distally and proximally targeting synaptic activity also affect the statistical properties of the fluctuations. The effects of synaptic input and its dendritic integration on somatic variables can be investigated theoretically using cable theory (Tuckwell et al., 2002) and will be the focus of a future communication.

Because the spike initiation site lies electrotonically close to the soma (Debanne et al., 2011), we assume that those three purely somatic variables will define the firing rate uniquely. In this study we investigate the firing response in terms of those somatic variables (illustrated in Figure 1).

We therefore designed a stimulation protocol to reproduce awake-like dynamical state at the soma and investigate the firing response in this three dimensional space. We evaluate the parameters of stochastic current and static conductance that would result in a particular configuration of the V_m fluctuations (μ_V , σ_V and τ_V) for passive membrane using a single-compartment approximation (Kuhn et al., 2004). This procedure allows to focus on how active currents convert fluctuations into spikes. Another advantage of this approach is that it naturally rescales the input with respect to the individual cellular properties (R_m , C_m and E_L) and therefore allows a cell-by-cell comparison. In addition, we investigated domains of the dimensionless variable $\tau_V^N = \tau_V / \tau_m^0$ instead of absolute values for membrane time constant τ_V to account for scaling of the synaptic inputs with membrane area (Equation 16 in Methods VI.7).

IV.2 Template for the firing rate response of single neurons

A key challenge for the *in vitro* characterization of input-output relationship is to extract a reliable quantitative estimation of its functional form from a limited number of experimentally sampled points. One approach consists in fitting the response to the formula derived from a specific theoretical model, such as leaky integrate-and-fire neuron (Rauch et al., 2003; ?). This strategy has three drawbacks: 1) the complexity of the analytical formula requires a careful numerical determination and thus render fitting procedures non trivial, 2) it does not generalize easily to biophysically-realistic synaptic input (e.g. reproducing synaptic dynamics, see Brunel and Sergi (1998)) and 3) the low number of parameters of simple theoretical models (e.g. a single spike threshold for the leaky integrate-and-fire model) imposes that the membrane parameters (e.g. leak conductance and membrane capacitance) are free parameters to have enough degrees of freedom.

We propose here a different strategy: we introduce a flexible analytical template fully determined by membrane parameters, which are experimentally measured, and some free parameters, which can be fitted using a simple two-step minimization procedure.

The basis for the template rely on a simple estimate, analogous to Amit and Brunel (1997), for the firing rate response of the LIF model:

$$\nu_{\text{out}} = \frac{\Pr(V > V_{\text{thre}})}{\tau_V} = \frac{1}{2\tau_V} \cdot \text{Erfc}\left(\frac{V_{\text{thre}} - \mu_V}{\sqrt{2}\sigma_V}\right) \quad (1)$$

It is obtained heuristically by splitting the time axis in bins of length τ_V , the spiking probability is then the probability that the membrane potential is above the threshold V_{thre} (see Methods VI.10). In comparison with earlier approach (Amit and Brunel, 1997), we take here the global autocorrelation time instead of the membrane time constant. We used this approximation as a baseline trend for the firing rate response and the properties of an individual cell will be described by deviations from this baseline behavior.

We found that those deviations could be accurately accounted for by replacing the hard threshold of the approximation V_{thre} by a linear phenomenological threshold:

$$V_{\text{thre}}^{\text{eff}}(\mu_V, \sigma_V, \tau_V^N) = P_0 + P_\mu \frac{\mu_V - \mu_V^0}{\delta\mu_V^0} + P_\sigma \frac{\sigma_V - \sigma_V^0}{\delta\sigma_V^0} + P_\tau \frac{\tau_V^N - \tau_V^{N0}}{\delta\tau_V^{N0}} \quad (2)$$

The quantities: $(\mu_V^0, \delta\mu_V, \sigma_V^0, \delta\sigma_V, \tau_V^{N0}, \delta\tau_V^N)$ are constant rescaling factors of the $(\mu_V, \sigma_V, \tau_V^N)$ space, see Methods VI.11.

A practical advantage of the template (Equation 1) is that, given some data $\nu_{\text{out}}(\mu_V, \sigma_V, \tau_V^N)$, we can invert the equation to get the phenomenological threshold as a function of the output firing rate:

$$V_{\text{thre}}^{\text{eff}}(\nu_{\text{out}}, \mu_V, \sigma_V, \tau_V^N) = \sqrt{2}\sigma_V \text{Erfc}^{-1}(2\tau_V^N \tau_m^0 \nu_{\text{out}}) + \mu_V, \quad \forall \nu_{\text{out}} > 0 \quad (3)$$

Where Erfc^{-1} is the inverse of the complementary error function.

We used this property to design the final fitting procedure: given some data $\nu_{\text{out}}(\mu_V, \sigma_V, \tau_V^N)$, we calculate the phenomenological threshold data using Equation 3 and fit coefficients $P_0, P_\mu, P_\sigma, P_\tau$ by linear regression. Then starting from those coefficients we perform a non-linear least-square fitting. Those two steps guarantee that the non-linear optimization starts from a good initial guess and ensures that the gradient-descent method converges close to the global minimum.

IV.3 Firing rate response of theoretical models

We start by demonstrating the accuracy and flexibility of this phenomenological description on the firing rate response for various theoretical models (Figure 2).

The model considered in this study is the inactivating adaptative exponential and fire (Methods VI.9), which extends the model of Brette and Gerstner (2005) by adding an inactivation mechanism (Platkiewicz and Brette, 2011). Several widespread theoretical models are special cases of this model: the leaky integrate and fire (LIF), the exponential integrate and fire (EIF, Fourcaud et al. (2003)), the inactivating leaky integrate and fire (iLIF, Platkiewicz

Table 1: Fitted coefficients of the linear phenomenological threshold for the theoretical models shown in Figure 2

model	P_0 (mV)	P_μ (mV)	P_σ (mV)	P_τ (mV)
LIF	-49.74	1.71	0.31	-0.51
EIF	-46.9	1.69	1.47	-3.6
sfaLIF	-49.49	4.29	3.91	0.56
iLIF	-46.11	2.33	-1.06	3.62
iAdExp	-48.78	4.72	5.25	-1.35

and Brette (2011)). We also define a LIF model with spike-frequency adaptation only (sfaLIF).

We show on Figure 2 that the template is able to describe the firing rate response of those various theoretical models. The impact on firing of those different biophysical properties of those models could all be accurately captured by differences in the linear phenomenological threshold (Figure 2D).

We compared the four-parameter description to simpler and more complex models in which the phenomenological threshold is: constant (1 parameter), linear function (4 parameters) or second-order polynomial of μ_V, σ_V and τ_V^N (10 parameters). The goodness to fit of the single-parameter description was $84.6\% \pm 8.9$; it increased to $99.0\% \pm 0.5$ for the four-parameter description; and then to $99.6\% \pm 0.2$ for the quadratic phenomenological threshold with 10 parameters. We conclude that the four-parameter description offers a good compromise between goodness-to-fit and number of parameters and will consequently avoid over-fitting of the experimental data.

In absence of active mechanisms, membrane potential fluctuations are statistically identical in all theoretical models (by design, they are the same leaky RC circuit). The active mechanisms may nonetheless have an impact on the membrane potential fluctuations themselves and will, by this mean, impact the firing response. In our description, those effects are captured in the dependency of phenomenological threshold on input variables. For example, the stationary spike-frequency adaptation level induces a net hyperpolarizing current, which, in our description, leads to an increased phenomenological threshold (sfaLIF vs. LIF in Figure 2D).

IV.4 Link between the biophysical properties and the characteristics of the firing rate response in theoretical models

To capture the particular features determining the properties of neuronal computation in the fluctuation-driven regime, we now turn to analyzing firing rate responses of the models. We define four simple quantities that provide a reduced description of the response of a single neuron: a mean excitability (mean phenomenological threshold) and average sensitivities to variations of mean μ_V , standard deviation σ_V and speed of the fluctuations τ_V^N . These quantities were average for all combination of the three input variables consistent with awake-like conditions (low-rate, 1 - 15 Hz, fluctuation-driven regime, \mathcal{D} domain in

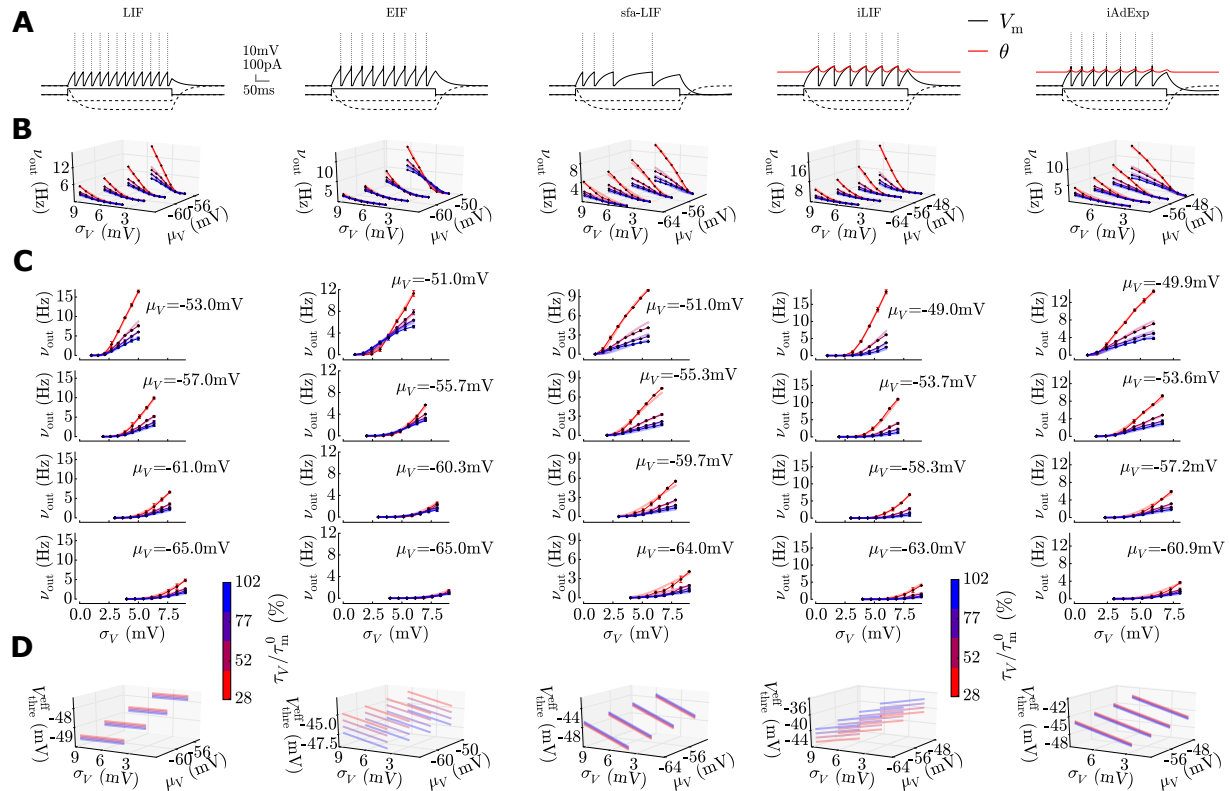


Figure 2: The analytical template (Equations 1 and 2) can capture the firing rate response of various theoretical models. Shown for the Leaky Integrate and Fire model (LIF) with $V_{thre}=-47\text{mV}$ (kept for all following models), the EIF with $k_a = 2\text{mV}$, the sfaLIF with $b = 20\text{pA}$, the iLIF with $a_i = 0.6$ and the iAdExp model that combines all the previously mentioned mechanism with $k_a = 2\text{mV}, b = 6\text{pA}, a_i = 0.6$. **(A)** Response of the models to a current step. Plain line: response to depolarizing current step, dashed line: response to hyperpolarizing current step. For the iLIF and iAdExp models, we show in red the dynamics of the threshold $\theta(t)$. **(B)** Firing rate response in the (μ_V, σ_V) space. Color indexes variation of the global autocorrelation ratio τ_V/τ_m^0 . **(C)** Projections along the standard deviation σ_V axis for different mean polarization levels μ_V . Data (points) and fitted analytical template (thick transparent lines). Note the shifts in the scanned μ_V domain to reach a comparable firing range despite a reduced excitability (see main text). **(D)** Phenomenological threshold V_{thre}^{eff} that leads to the fitted firing response, the coefficients of the linear functions can be found in Table 1.

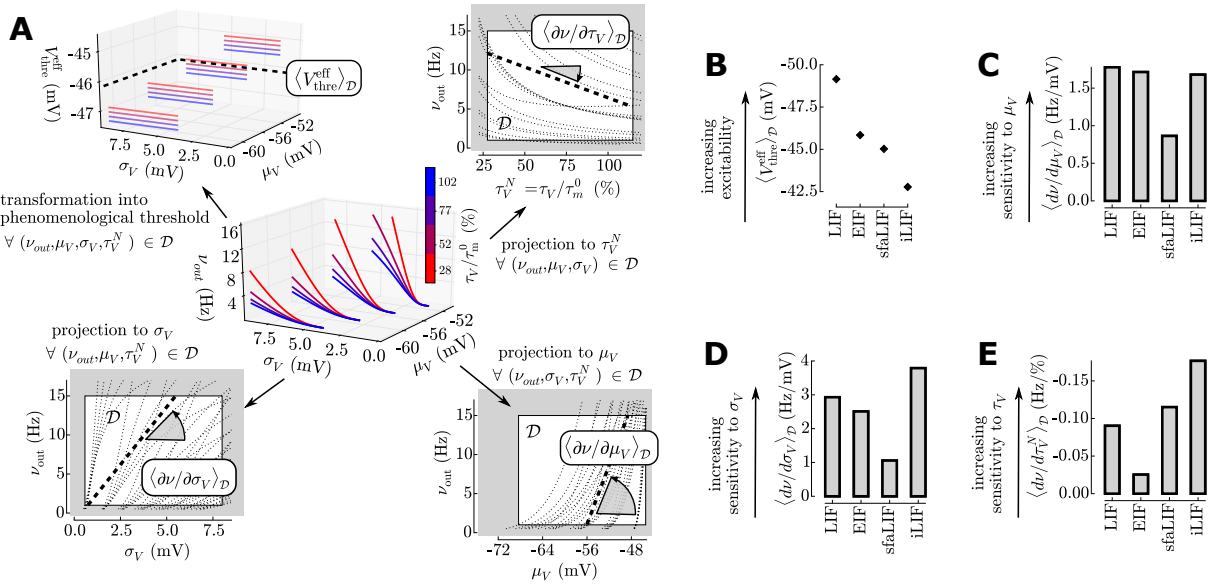


Figure 3: Extracting the mean properties of a single neuron response: excitability and sensitivities to the variables of the *fluctuation-driven* regime. (A) Illustration for the LIF model. From the fitting procedure we obtain an analytical description of the firing rate response (center plot). We focus the analysis on the domain \mathcal{D} of the low rate fluctuation-driven regime (see main text IV.4), its extent is delimited by the white square in the bottom and top-right insets. The mean phenomenological threshold in the \mathcal{D} domain quantifies the excitability (top left: large dashed line). Then for each variable (top right: τ_V^N , bottom left: σ_V , bottom right: μ_V), we show the projections of the firing response along this dimension for different combinations of the two other variables within the \mathcal{D} domain (dotted lines). The mean derivative (represented by arc angle and large dashed line) with respect to the variable in x-axis over different combinations of the remaining variables quantifies the mean sensitivity to this variable. (B) Excitabilities for the LIF, EIF, sfaLIF and iLIF models (parameters as in Figure 2). (C) Mean sensitivities to μ_V . (D) Mean sensitivities to σ_V . (E) Mean sensitivities to τ_V/τ_m^0 for the four models.

Figure 3).

The LIF model provides a basic picture for the firing rate response (see LIF in Figure 2 and Figure 3A). Spiking in the LIF model increases with mean depolarization and the standard deviation (bottom panels in Figure 3A), while it decreases with the global autocorrelation time (top right panel in Figure 3A). More sophisticated biophysical mechanisms implemented in the considered theoretical models (exponential activation, adaptation, etc.) affect those baseline characteristics. First of all, such mechanisms suppress spiking and therefore reduce the mean excitability of all the models (Figure 3B). The effect on average sensitivities is more complex.

The substitution of the hard threshold of LIF with an exponential function in EIF imitates the gradual opening of sodium channels in time. This property has a very strong impact on the dependency on the speed of the fluctuations (Figure 3E). In contrast to LIF, fast fluctuations do not lead to an increase of spiking. This effect, which occurs due to the inability of smooth sodium activation curve to extract fast varying fluctuations (Fourcaud et al., 2003), is well captured by our analysis: the sensitivity to τ_V^N is much reduced for the EIF with respect to the LIF model.

The spike frequency adaptation of sfaLIF reproduces the effect of a calcium-dependent potassium current (Im current) that tend to hyperpolarize neocortical pyramidal neurons at each spike occurrence (McCormick et al., 1985). This is an effect that attenuates firing and because it is proportional to firing itself we expected it would reduce the dependencies to all variables. Indeed the sensitivities to μ_V and σ_V are strongly attenuated with respect to LIF (Figure 3C-D). In contrast, the sensitivity τ_V^N is only mildly affected. The temporal dynamics of the hyperpolarizing current ($\tau_W=500\text{ms}$) impedes short inter-spike intervals in the output spike train, consequently slow fluctuations are more strongly damped than fast fluctuations which restores the sensitivity to τ_V^N (Figure 3E).

The iLIF model reproduce the fast inactivation properties of sodium channels (see ? for a review). Close to threshold, sodium channels tend to rapidly inactivate ($\tau_{\text{inact}}=5\text{ms}$). This mechanism clearly favors fast and high amplitude fluctuations, which allow to trigger a spike before the channels become unavailable. Indeed, the sensitivity to σ_V and τ_V^N is strongly enhanced (see Figure 3D-E).

IV.5 Response of juvenile mice layer V pyramidal neurons *in vitro* with the perforated-patch technique

We now use the above analytical tools to determine experimentally firing rate responses *in vitro*. Scanning the response of neocortical neurons in the fluctuation-driven regime is experimentally challenging because it is characterized by an irregular firing at low rates ($\sim 0.1\text{-}20\text{ Hz}$). To obtain a meaningful estimation of the firing rate response we need long and stable recordings (Rauch et al., 2003; ?). Both to obtain this stability and to ensure the integrity of the intracellular medium (in particular to maintain a physiological Ca^{2+} dynamics), we chose the *perforated*

patch technique (Rae et al., 1991; Lippiat, 2009), in which electrical access is obtained by inserting a conducting pore (Amphotericin B protein permeant only to monovalent ions) in a patch of membrane (Wendt et al., 1992; Kyrozi and Reichling, 1995). Although the technique may sometimes limit the quality of the electrical access to the cell, we achieved very low ratios between the access resistance and the membrane resistance ($4.7 \pm 2.6\%$, see also Rae et al. (1991)), thus allowing for reliable use of the *dynamic-clamp* technique (?).

We monitored the stability of recordings by means of three quantities: 1) the resting membrane potential, 2) the membrane resistance and 3) the variations of the firing rate probability and formulated strict criteria for the stability of the recordings (see Figure 4E).

The resulting dataset contains $n=30$ cells, it totals to 65455 spikes fired at an average frequency of 3.62Hz, i.e. within the low-rate, fluctuation-driven regime defined above (1 - 15 Hz). This relatively large amount of data was necessary to extract the biophysical relations between the fluctuations properties and the stationary firing rate.

We investigated whether the combination of the analytical template (and its fitting procedure) with our experimental recording protocols was able to produce a reliable characterization of the firing rate response of layer V neocortical neurons in juvenile mice visual cortex.

For each of the $n=30$ cells, we obtained a given scan of the $\mu_V, \sigma_V, \tau_V^N$ space and applied our fitted procedure. We show the data and the fit for four examples in Figure 5. The goodness-to-fit of our template was high (goodness-to-fit of $88.6\% \pm 9.4$, compared to only $38.4\% \pm 35.3$ for the constant threshold and $90.6\% \pm 9.2$ for the quadratic phenomenological threshold), the small divergence is due to intrinsic irregularity of the low-rate spike process (sampled over 5 s per episode, Figure 4E). In spite of this variability, the linear threshold averages the intrinsic firing irregularity and produces a reliable characterization of the firing rate response.

To quantify the robustness of the experimental characterization, we splitted the measurements into two sets and investigated whether the first half of data would give the same phenomenological threshold as the second half. We found a good agreement if the number of scanned configuration of input space (μ_V, σ_V, τ_V) was $n_{\text{points}} \geq 70$ (Pearson correlations, $c > 0.8$ and $p < 1e-5$ for the correlations between first and second half of data, Figure 5B). The high Pearson correlations between the response characteristics in the two subsets indicates that the characterization is robust for $n_{\text{points}} \geq 35$ scanned combinations of input parameters. Among the 30 cells used for further analysis, the cell with the minimum number of points had $n_{\text{points}} = 42$ scanned combinations meeting the above criterion for the robustness.

IV.6 Single neurons show strongly heterogeneous firing rate responses

A striking feature in the response of the recorded cells is the differences in their response.

We illustrate this property on the four examples shown in Figure 5A. Cells 1 and 4 show a very strong dependency

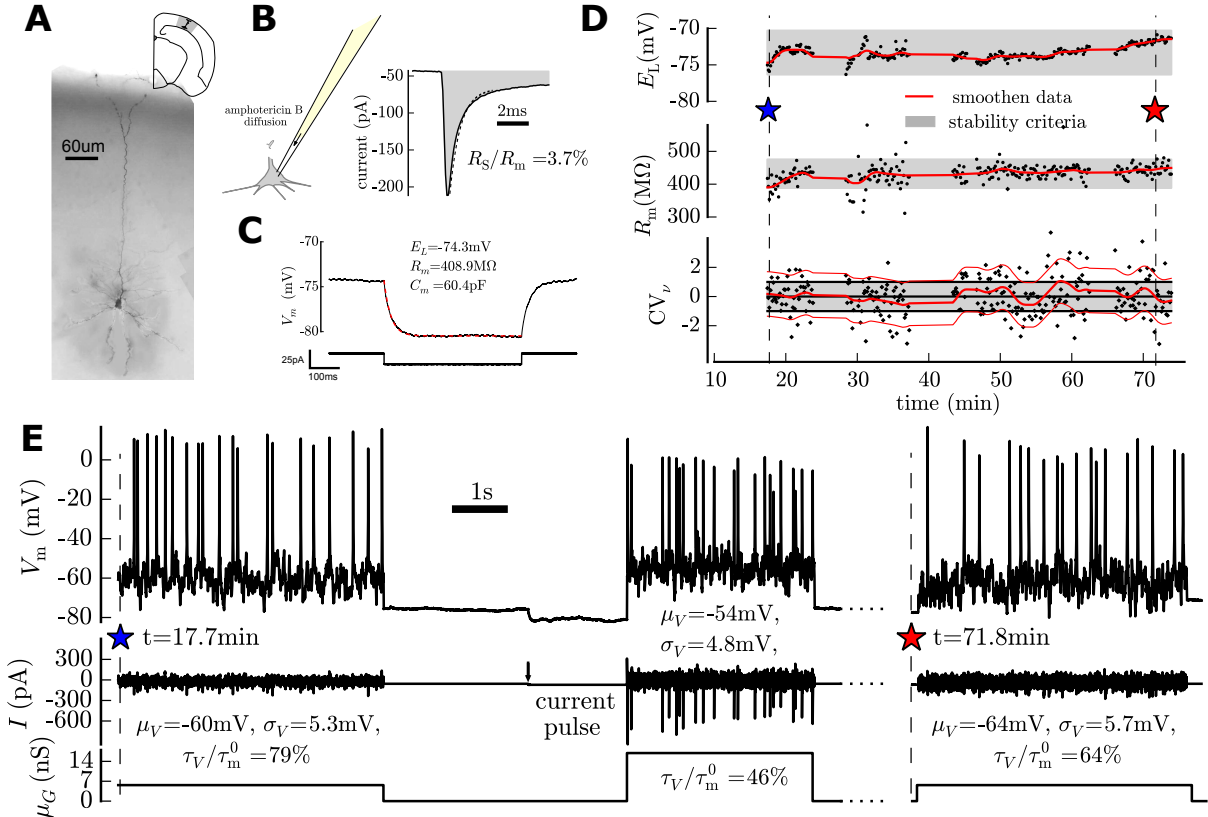


Figure 4: The exploration of a physiologically-relevant space in layer 5 pyramidal neurons of juvenile mice. From **B** to **E**, an example of a single cell. (**A**) A typical layer 5 pyramidal neuron in the primary visual cortex of juvenile mice. Picture from additional experiments: marking with 2% Biocytin (Sigma Aldrich) in whole cell configuration. (**B**) After diffusion of the perforant molecule toward the patch of membrane, a step voltage clamp protocol estimates the quality of the seal and perforation (see details in the Methods VI.2). (**C**) A step current clamp protocol estimate the passive membrane properties. Those properties are used by the stimulation protocols to constrain the V_m fluctuations (see Methods VI.7). (**D**) All along the recording, we monitor the cellular properties: the resting membrane potential E_L , the membrane resistance R_m and the variations of the firing rate with respect to the stationary behavior CV_ν (see details in the main text IV.5 and in the Methods VI.8). The smoothed data (red curve) show the global trend, it removes the measurement error due to the short sampling time for R_m and E_L (see **E**), for CV_ν , it removes the intrinsic spiking irregularity. For the CV_ν curve we have added the standard deviation (mean \pm std in red) for comparison with a stationary Poisson process (mean \pm std in black). (**E**) Sample of the membrane potential V_m , the injected current I and the total conductance μ_G at the beginning of the recording (left, $t=17.7\text{min}$, blue star in **D**) and one hour after (right, $t=71.8\text{min}$, red star in **D**). Within an episode, we scan one combination of the $(\mu_V, \sigma_V, \tau_V^N)$ variables. For example, the middle episode corresponds to the most depolarized level μ_V (hence the lower spike amplitude due to Na inactivation) with the fastest fluctuations τ_V^N (i.e. an high input conductance μ_G , also shunting the spikes, see the strong opposite current) and an intermediate variance σ_V . In between the two first episodes, one can see rest period (to monitor E_L) followed by a current pulse (to monitor R_m).

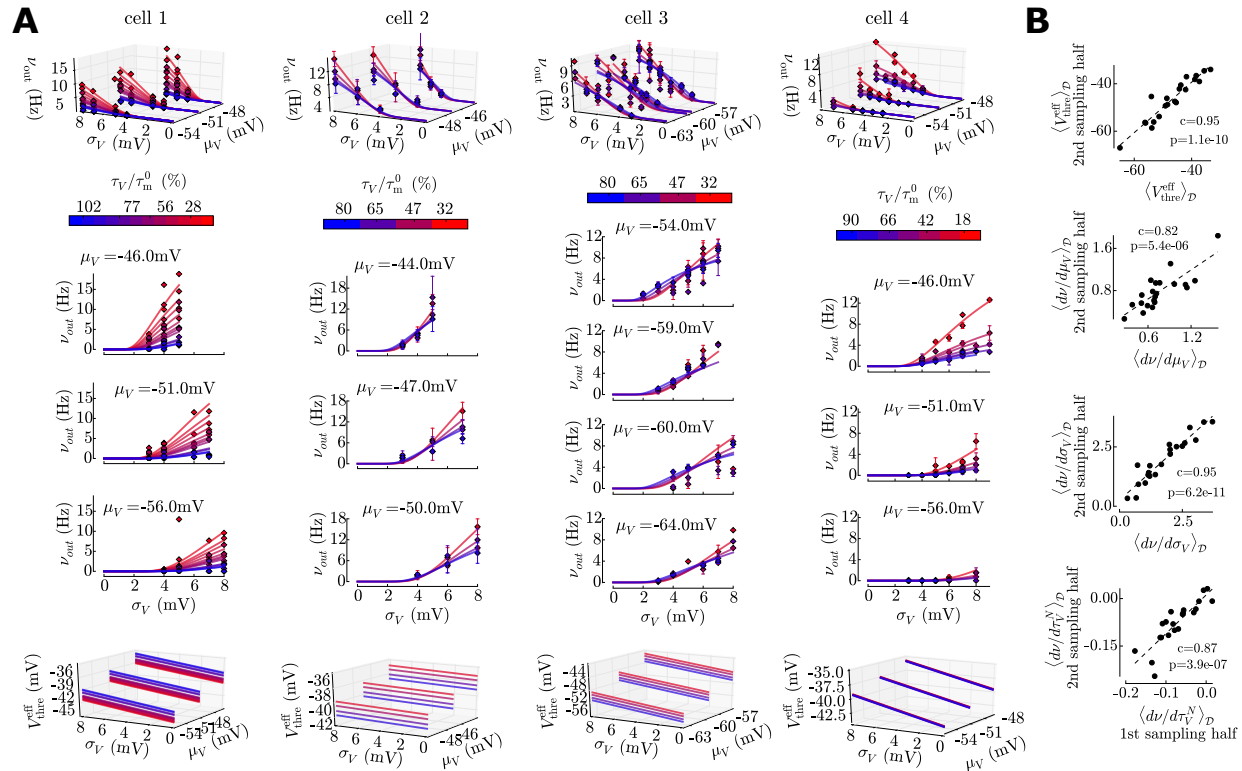


Figure 5: Characterization of the firing rate response of the recorded neocortical pyramidal neurons. (A) Four examples of the firing rate response of single neurons, data (diamonds, error bars indicate variability estimated as the standard deviation from responses to multiple trials where available) and fitted template function (plain line), the cells are indexed from 1 to 4 to identify them in the heterogeneity analysis (Figure 6). (B) For 21 neurons scanned with at least of 70 different combinations of input statistics, we split the dataset into two and investigate the similarity of the coefficients between the two subsets. The relatively high and significant ($p < 0.05$, Pearson correlation) correlation coefficients between characterizations in the first and second datasets indicate a robust characterization of the firing rate response.

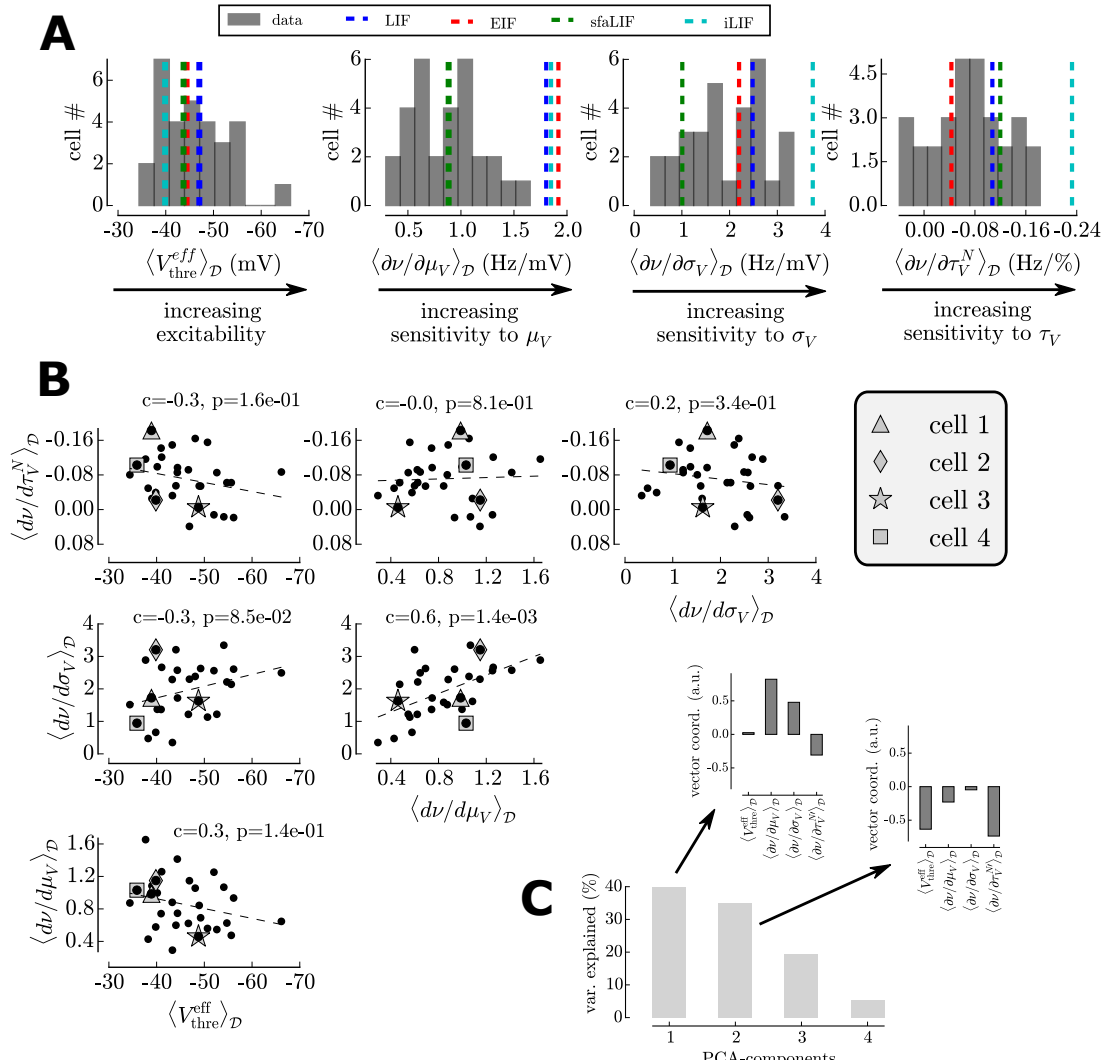


Figure 6: Heterogeneity and underlying structure of the firing response of neocortical cells (A) Histogram over recorded cells of the mean excitabilities and sensitivities to the variables of the fluctuations. The dashed color lines show the values of theoretical models for comparison. (B) Scatter plot of the mean excitability and sensitivities to the variables of the fluctuation-driven regime, we highlighted the cells shown in Figure 5 with larger markers. (C) Principal component analysis, in the inset, the vector coordinates of the two first components

on speed of the fluctuations τ_V , whereas cells 2 and 3 are almost insensitive to this parameter (different colors in 5A). The dependency on the standard deviation of fluctuations σ_V is steeper for cell 2 than for 3 and 4. Also the sensitivity to μ_V seems to be variable, a 10 mV depolarization has stronger effect on responses of cell 4 than 3. Finally, the cell excitabilities are also highly variable, so that they reach the 1-15Hz firing range at various depolarization levels (e.g. compare cell 2 and 3). Similar differences are present in all recorded pyramidal cells (Figure 6A).

This strong heterogeneity raises the question whether there is an underlying structure in the variations of the characteristics of the firing rate response and how could it be explained by diverse biophysical mechanisms.

First, when plotted in four-dimensional space of the firing response characteristics the data did not seem to distribute into distinct clusters (Figure 6B). Presented on two dimensional projections, the excitability and sensitivities to input variables of different cells co-vary (Pearson correlation, c , Figure 6B). We then looked for the four-dimensional structure of those co-variations in the response characteristics by means of a principal component analysis (Figure 6C). No single co-variation of the sensitivities could explain a strong percentage of the observed heterogeneity, suggesting that the correlation structure is weak.

Nonetheless, two vectors explained 75% of the variations in the data. The first vector corresponds to a co-variation of the sensitivities to mean and amplitude of the fluctuations. This co-variation can be achieved in the sfaLIF model, varying the weight of spike frequency adaptation concomitantly varies the sensitivities to μ_V and σ_V (Figure 7C). The second vector corresponds to a co-variation of a decrease in the excitability and an increase in the sensitivity to the speed of the fluctuations. The variability in excitabilities is quite remarkable, to reproduce it in the LIF model one needs variations of the threshold V_{thre} that spans nearly 15 mV (see Figure 7). The variability in the sensitivity to τ_V covers a wide range of parameters in theoretical models, from an EIF model with a smooth curve ($k_a=2\text{mV}$) to a strongly inactivating iLIF model ($a_i=0.7$). Increasing the threshold while increasing the impact of sodium inactivation and increasing the sharpness of the sodium activation curve would therefore reproduce the second component of the principal components analysis.

V Discussion

We studied systematically the firing rate response of different neuronal models as well as *in vitro* layer V pyramidal cells as a function of the three variables composing our definition of the *fluctuation-driven* regime.

Compared to previous studies (La Camera et al., 2008), we focused on the low rate regime and we extended the domain of somatic *in vivo*-like conditions. In particular, we investigated the dependency on the firing rate for high somatic conductance and low autocorrelation time of the membrane potential fluctuations. Scanning the response to low autocorrelation time allowed to highlight the impact of sodium inactivation because this is the regime where

the temporal dynamics of this features is likely to play ($\tau_{\text{inact}} \sim 5\text{ms}$).

We formulated a two-step procedure to circumvent the issue of spatially distributed inputs in neocortical neurons where the intermediate quantities are the properties of the V_m fluctuations at the soma. Other investigators studied the response to the noisy current input properties at the soma and then addressed the problem of how dendritic integration shape the properties of this current (La Camera et al., 2008; Giugliano et al., 2008). Our approach can be seen as a way to include the mean conductance effect due to changes in background synaptic activity. The reason we presented the data as a function of the V_m fluctuations properties and not the quantity that the experimentalist actually controls (the current and the conductance) is that it allows to compare individual cells and that the spiking response is dominated by subthreshold integration effects, e.g. for a same variance of input current, an increasing conductance would decrease the V_m fluctuations amplitude by shunting effects (Kuhn et al., 2004). The effects of the spike-related mechanisms are then difficult to de-intricate from those subthreshold effects. Here, we used calculus to design a stimulation protocol that allows to control the fluctuations and therefore to focus on understanding the single neuron computation on top of the fluctuations properties.

Starting from a simple approximation, we showed that bringing the problem into a phenomenological threshold space was a simple way to describe the firing rate response of neocortical neurons. Other investigators already reported that a shift in the threshold was a convenient way to account for increasing biophysical complexity (Brunel and Sergi, 1998; Platkiewicz and Brette, 2010). Unlike the two mentioned studies, the form of our phenomenological threshold was not derived mathematically (it was arbitrarily taken as linear) but we believe that the descriptive power of this very simple form further confirms the idea that the threshold space is a convenient space to work in.

We showed that this template is able to describe the response of neuronal models of varying complexity. We then used this simple description to design a robust characterization of the firing rate response of single neurons experimentally. This approach, combined with the long and stable recordings provided by the perforated patch technique, was our way to circumvent the experimental and theoretical difficulties of assessing a relevant firing rate response in a low rate irregular firing regime.

We now discuss the biophysical mechanisms relevant for the firing rate response of layer V pyramidal cells in juvenile mice visual cortex.

First, spike frequency adaptation was shown to be an important mechanism to the firing rate response. Notably, all models lacking spike frequency adaptation (LIF, EIF, iLIF) had a sensitivity to μ_V higher than all recorded cell. This mechanism is therefore crucial to reproduce the attenuated sensitivity to depolarizations of layer V pyramidal cells in mice visual cortex.

Many cells showed a weaker sensitivity to the speed of the fluctuations than the LIF model ($n=20$ out of 30). This could be reproduced in theoretical models by implementing a smoother activation curve for the

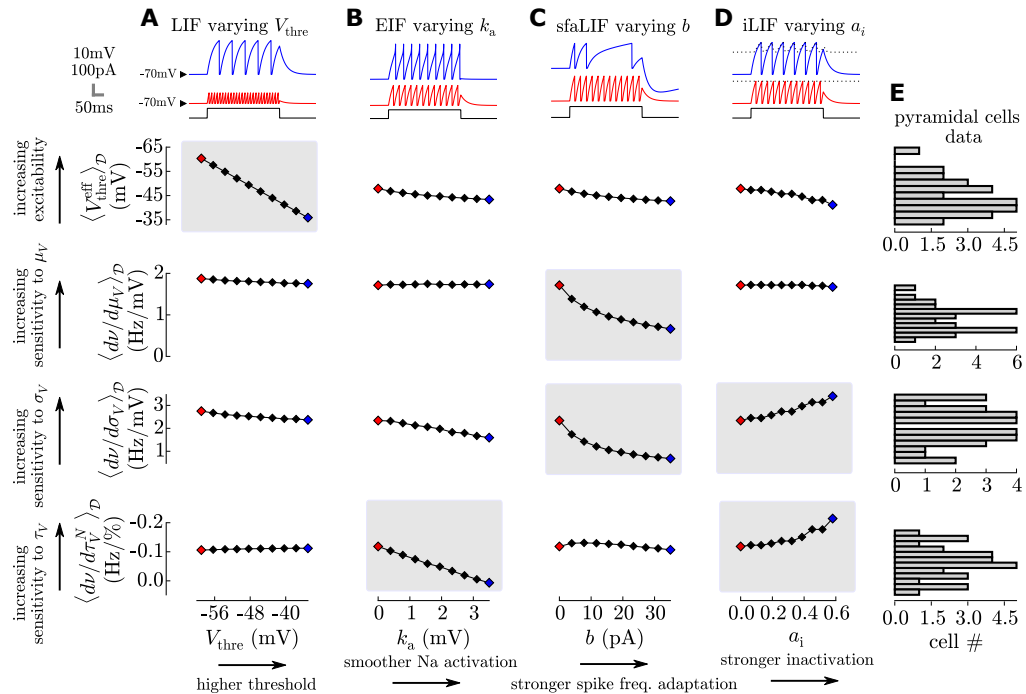


Figure 7: Variations in the expression of biophysical mechanisms explain the observed cellular heterogeneity in their firing rate response. (A) Increasing the threshold V_{thre} of the LIF model. Note that this only affects the excitability and negligibly the sensitivities to μ_V , σ_V and τ_V^N . (B) Decreasing the sharpness of the sodium activation curve in the EIF model, $k_a=0\text{mV}$ corresponds to the LIF model, $k_a=3.7\text{mV}$ corresponds to a very smooth activation. Note the strong impact on the sensitivity to τ_V^N . (C) Increasing spike frequency adaptation in the sfaLIF model, $b=0\text{ mV}$ corresponds to the LIF model, $b=35\text{pA}$ corresponds to a strongly adapting model. Note the concomitant variations of the sensitivities to μ_V and σ_V . (D) Increasing sodium inactivation in the iLIF model, $a_i=0$ corresponds to the LIF model, $a_i=0.7$ corresponds to a strongly inactivating model. Note the strong impact on the increase in sensitivity to σ_V and τ_V^N . (E) Histogram of the data from the $n=30$ neurons.

sodium channels (EIF models of varying sharpness). This observations contrasts with reports from studies in more mature pyramidal neurons in rat neocortex (?; Ilin et al., 2013), where it was found that pyramidal cells could have a very sharp activation curve that would enable them to extract very fast input. Nevertheless, even at the soma, the neurons of our recordings show a rather smooth activation curve: $k_a \sim 1.5$ mV (not shown) from the dynamic I-V curve analysis (Badel et al., 2008) rendering this possibility unlikely.

Surprisingly some cells showed a stronger sensitivity to the speed and amplitude of the fluctuations than the LIF model ($n=10$ out of 30). By penalizing slow and low amplitude fluctuations, sodium inactivation seem to be able to explain this phenomena. Our observation is thus analogous to the phenomena described in ? for pyramidal cells in rat CA1, where the authors found that a high conductance state (corresponding to fast fluctuations in our study) could evoke more spikes than a low conductance state (slow fluctuations here). Their study provides evidence for the role of fast sodium inactivation in the sensitivity to the speed of the fluctuations and is therefore compatible with our modeling results. Because of its role in promoting large amplitude and/or fast fluctuations, sodium inactivation seems to be a key property in shaping the input-output properties of layer V pyramidal cells in the fluctuation-driven regime.

Finally, we did not discuss the impact of other subthreshold non-linearities usually present in pyramidal cells such as the Ih current. This mechanisms is weakly expressed in the pyramidal cells of our recordings (see response to current steps in Figure 4C). Nevertheless, we investigated its effect on the firing response (not shown). Because of its high pass filtering behavior, it would have an effect very similar to the one of sodium inactivation: penalizing slow fluctuations and therefore increasing the sensitivity to τ_V .

In conclusion, our study shows that the spiking response of cortical neurons is highly inhomogeneous in juvenile mice visual cortex. Because we see no evidence for any type of invariance of cellular responses (after rescaling by membrane parameters), this aspect of cellular heterogeneity should then be considered as an additional component to the diversity in cell size and shape classically reported in cerebral cortex.

Those diverse firing responses will consequently strongly affect population rate dynamics in the low rate fluctuation-driven regime. Such results and measurements should be incorporated into mean-field descriptions of cortical dynamics to understand the properties emerging at the network level , which constitute the main perspective for future continuation of the present work.

VI Material and Methods

VI.1 Experimental preparation

Experimental procedures with animals were performed following the instructions of the European Council Directive 2010/86/EC and its French transposition (Décret 2013/118). Swiss wild-type mice of either sex, 8–13 days old, were anesthetized with inhaled isoflurane and decapitated, their brain

was rapidly removed and immersed in cold “cutting” solution ($\sim 4^\circ\text{C}$) containing the following (in mM): 110 Choline Chloride, 2.5 KCl, 1.25 NaH₂PO₄, 26 NaHCO₃, 8 MgCl₂, 1 CaCl₂, 10 glucose, pH equilibrated to 7.3 with O₂/CO₂ (95%/5%). Coronal slices (300 μm thick) were prepared with a vibratome (Leica VT1200 S, Leica Microsystems) and stored at room temperature in oxygenated aCSF containing the following (in mM): 126 NaCl, 2.5 KCl, 1.5 NaH₂PO₄, 26 NaHCO₃, 2 MgCl₂, 2 CaCl₂ and 10 glucose, pH 7.4. The slices were then transferred to the recording chamber (perfused with the same solution) where the temperature was maintained at 34°C. Slices containing primary visual cortex were taken as the first four slices containing brain cortex starting from the most caudal one.

VI.2 Electrophysiological recordings

We performed intracellular recordings of visually identified pyramidal cells located in the layer V of mice cortex using the perforated patch technique.

Patch electrodes (tip resistance: 1.5–2.5 M Ω) were pulled on a Sutter P-1000 apparatus (Sutter Instruments) and filled in a two step procedure. The pipettes were pre-filled with a solution containing the following (in mM): 130 K-Gluconate, KCl 7, NaCl 1, MgCl₂ 4, HEPES 10, pH adjusted to 7.3 with KOH (osmolarity 260 mOsm). The pipette was then back-filled with the same solution to which was added Amphotericin-B (Sigma Aldrich) previously dissolved in DMSO, the final concentration of Amphotericin-B was 60 μM . The reason for this two step procedure is to allow a current flow out of the pipette (to preserve the tip from dirt) without pouring the perforant onto the target cell during the pipette approach. The perforation could therefore happen only after diffusion of Amphotericin-B through the “clean” solution, this usually took 5–10 minutes after the pipette filling, thus allowing the cell-attached configuration to form in absence of the perforant molecule.

We recorded from $n=30$ cells. After perforation, the access resistance R_S was $14.7\text{M}\Omega \pm 6.9$. This value was plugged in into the amplifier-build bridge compensation system during the current-clamp recordings. At -75 mV, the recordings exhibited a leak current of $-31.9\text{ pA} \pm 26.8$ (minimum observed resting potential: -76 mV), this current value was then set for each neuron as the holding current during the recording. Recorded pyramidal cells had an input resistance R_m of $355.9\text{ M}\Omega \pm 184.1$ and a membrane time constant at rest of : $31.4\text{ms} \pm 12.0$. Recordings lasted $36.7\text{ min} \pm 20.9$. In the absence of current injection, cells presented a quiescent activity.

The liquid junction potential was measured to be 6 mV and membrane potential recordings were corrected accordingly. Note that there might be anyway an unknown constant shift in the voltage value because the Amphotericin-B pores are selective channels (so that a non-zero reversal potential could appear if the cellular medium and our pipette medium are different). The absolute values of the membrane potential presented here should therefore be interpreted carefully (but this would only affect the $\langle V_{\text{thre}}^{\text{eff}} \rangle_D$ quantity reported in this study).

VI.3 Measuring firing rate

We measured the firing rate simply by counting spikes over a fixed time window. Spikes were detected as upward crossings of -20mV. The first 100ms we removed to avoid transient effects associated to the membrane potential rise. The duration of the stimulation was usually 5s, therefore the minimum (non zero) rate was 0.2 Hz. Also an online analysis was counting

spikes and the stimulation was stopped when ~ 20 spikes were reached (see in Figure 4E, the middle episode is shorter than the two other ones), this to avoid spending too much recording time in the high firing rate range.

VI.4 Dynamic-clamp

Our dynamic-clamp system consists of an Intel Quad-Core computer equipped with an acquisition card (NI PCI-6251 ADC/DAC, Mseries, National Instruments) connected to the amplifier operating in current-clamp mode. The dynamic-clamp software is based on a custom ADC/DAC (analog-to-digital/digital-to-analog) program used for data acquisition and analysis [Elphy2, developed at Unité de Neurosciences, Information et Complexité (UNIC) by Gérard Sadoc] and interfaced with the NEURON simulator version 6.0 (Hines and Carnevale, 1997). NEURON was modified and recompiled to run under the INTIME (TenAsys), a Real Time Operating System running alongside Microsoft Windows. The recordings were performed using a Multiclamp 700B amplifier (Molecular Devices). Stimulation protocols were run in real time with the acquisition card at 10 kHz. Acquisition and filter frequencies were set at 10 and 4 kHz, respectively. An unfiltered copy of the membrane potential signal was feeding the *dynamic clamp* system.

VI.5 Single compartment approximation

Both for the experimentally recorded neurons and for the theoretical models, we will use the single compartment membrane equation. The passive properties of a neuron are therefore described by a leak conductance g_L , a capacitance C_m and a resting potential E_L . With an additional current $I(V, t)$, the membrane potential thus follows:

$$C_m \frac{dV}{dt} = I(V, t) + g_L (E_L - V) \quad (4)$$

Passive properties were fitted from the response to a hyperpolarizing current step for the recorded neocortical neurons in the subthreshold domain (around -75 ± 5 mV).

Though this approximation was found to be satisfactory (Figure 4C), monitoring possible deviations is important in this study as the approximation is used to shape the fluctuations of the membrane potential. We therefore performed a cell-by-cell quantification of the accuracy of the approximation as follows. We take the protocols that were used to determine the membrane properties: prior to each protocol, we recorded and averaged the response to 10 current pulses of ~ 500 ms and of $\Delta I \sim 15$ pA amplitude, not the (noisy) continuous monitoring presented in Figure 4. We average over trials the membrane potential response and fit an exponential curve to this mean response $V_{sc}^{fit}(t)$, we get a membrane time constant τ_m^0 and a membrane resistance R_m^0 . We define the residual trace as the normalized absolute difference between the fit and the trace :

$$\text{Res}(t) = \left| \frac{V(t) - V_{sc}^{fit}(t)}{R_m^0 \Delta I} \right| \quad (5)$$

Now we quantify the accuracy of the single-compartment approximation by taking the (normalized) integral over 7 membrane time constant of the residual trace.

$$C_{sc} = \int_{t_0}^{t_0 + 7\tau_m^0} \frac{dt}{7\tau_m^0} \text{Res}(t) \quad (6)$$

The two normalizations (by membrane resistance and membrane time constant) were performed to yield comparable quantities for different membrane parameters.

We investigated whether the quality of the approximation had an impact on the excitability and sensitivities presented in the Results, we found no significant correlations between those quantities and the quality of the recordings ($c < 0.2$ and $p > 0.2$ for all characteristics, Pearson correlations), thus suggesting that the results of our study were not impacted by deviations from the single compartment approximation.

VI.6 Global autocorrelation time

We present here a theoretical estimate for the speed of the membrane potential fluctuations.

In the case of a fluctuating synaptic input with temporal dynamics (e.g. resulting from a shotnoise of *exponential* synapses considered in this study, unlike the *delta* synapses considered in other studies, see Amit and Brunel (1997) for an example), the autocorrelation function is not an exponential function. Consequently, the resulting membrane fluctuations can not be characterised by a single time constant τ_V (see the inset in Figure 1). Nevertheless, the time constant taken from an exponential approximation of the normalized autocorrelation function corresponds to a first order description of the auto-correlation and will be the main contributor to the temporal dynamics of the fluctuations.

As a theoretical prediction for this *global autocorrelation* time, we take the half integral of the normalized autocorrelation correlation function:

$$\tau_V = \frac{1}{2} \int_{\mathbb{R}} d\tau \frac{A(\tau)}{A(0)} \quad (7)$$

where $A(\tau)$ is the autocorrelation function of the V_m fluctuations (see an example of $A(\tau)/A(0)$ in Figure 1). From shotnoise theory (?), we will obtain the power spectral density of the V_m fluctuations $P_V(f)$, so we re-express the global autocorrelation time as:

$$\tau_V = \frac{1}{2} \left(\frac{\int_{\mathbb{R}} P_V(f) df}{P_V(0)} \right)^{-1} \quad (8)$$

In this study, this formula reduces to a very simple form (see next section). Note that the relations presented in this paper rely on the following convention for the Fourier transform: $\hat{F}(f) = \int_{\mathbb{R}} F(t) e^{-2\pi f t} dt$.

VI.7 A stimulation to investigate the dependency on the variables of somatic fluctuations

We aim at reproducing the dynamical state at the soma in the fluctuation-driven regime by reproducing membrane potential fluctuations with the control of the mean μ_V , the standard deviation σ_V of the subthreshold fluctuations as well as a global autocorrelation time τ_V .

Our "input space" is already a response of the neuron, thus we need a stimulation that would reliably produce this response. There exists multiple types of input that would lead to a given set of the $(\mu_V, \sigma_V, \tau_V)$ variables. In the present study, to best characterize the dependency on those precise variables, we wanted a stimulation that would minimize the higher order terms appearing for realistic synaptic inputs, e.g. when injecting excitatory and inhibitory Ornstein-Uhlenbeck conductances (?; ?). We chose the following stimulation.

The mean membrane potential is achieved through a constant current input:

$$I_{\mu_V} = g_L (\mu_V - E_L) \quad (9)$$

Varying the speed of the fluctuations τ_V is achieved by changing the total input conductance at soma μ_G (an increasing conductance reduces the effective membrane time constant of the membrane, events are integrated faster and this renders fluctuations faster). The total conductance μ_G is changed by introducing a current I_{μ_G} of static conductance $g_S = \mu_G - g_L$ and of reversal potential μ_V :

$$I_{\mu_G}(V) = g_S (\mu_V - V) \quad (10)$$

We introduce here the effective membrane time constant $\tau_m^{\text{eff}} = C_m/(g_S + g_L)$.

An additional noisy current of zero mean creates the fluctuations around μ_V to control the standard deviation σ_V . This current is generated from two independent Poisson processes convolved with an exponential kernel: one excitatory, one inhibitory. They have the same presynaptic rate ν_{in} , the same time constant for the exponential decay τ_S and opposite current increments Q_I and $-Q_I$. This corresponds to the current I_{fluct} (t):

$$\tau_S \frac{dI_{\text{fluct}}}{dt} = -I_{\text{fluct}} + Q_I \left(\sum_k \delta(t_e^k - t) - \sum_k \delta(t_i^k - t) \right) \quad (11)$$

Where $\{t_e^k\}_{k \in \mathbb{N}}$ and $\{t_i^k\}_{k \in \mathbb{N}}$ are two sets of uncorrelated presynaptic events generated by the frequency ν_{in} .

A single excitatory or inhibitory post-synaptic potential event from this input will have the following time course:

$$PSP(t) = \pm \frac{Q_I \tau_S (e^{-\frac{t}{\tau_S}} - e^{-\frac{t}{\tau_m^{\text{eff}}}})}{g_L (\tau_m^{\text{eff}} - \tau_S)} \quad (12)$$

From shotnoise theory (?) (see also ? for an application similar to ours), we can obtain the power spectral density of the V_m fluctuations $P_V(f)$ as a response to the stimulation Equation 11:

$$\begin{aligned} P_V(f) &= \sum_{syn} \nu_{syn} \|P\hat{S}P(f)\|^2 \\ &= 2\nu_{in} \frac{Q_I^2 \tau_S^2 / \mu_G^2}{(1 + 4\pi^2 f^2 \tau_S^2)(1 + 4\pi^2 f^2 \tau_m^2)} \end{aligned} \quad (13)$$

The variance of the membrane potential fluctuations is the integral of the power density spectrum :

$$\sigma_V^2 = \int_{\mathbb{R}} P_V(f) df = \nu_{in} \cdot \frac{(Q_I \tau_S)^2}{(\tau_m g_L)^2 (\tau_S + \tau_m)} \quad (14)$$

And the global autocorrelation time takes the very simple form, see Equation 8 :

$$\tau_V = \frac{1}{2} \left(\frac{\int_{\mathbb{R}} P_V(f) df}{P_V(0)} \right)^{-1} = \tau_S + \tau_m \quad (15)$$

We rescale this relation with respect to the resting membrane time constant τ_m^0 :

$$\tau_V^N = \frac{\tau_V}{\tau_m^0} = \frac{\tau_S}{\tau_m^0} + \frac{g_L}{\mu_G} \quad (16)$$

Because the mean synaptic conductance μ_G should scale with the size of the membrane (because of the constant surfacic density of synapses), as does g_L (because of the constant surfacic density of leak channels), when the presynaptic bombardment increases, it is the rescaled quantity μ_G/g_L that increases. Therefore we investigated a fixed domain of the τ_V/τ_m^0 quantity.

Finally, the time- and voltage-dependent current $I(V, t)$ inserted into the membrane Equation 4 or injected via the dynamic-clamp technique takes the form:

$$\begin{cases} I(V, t) = I_{\mu_V} + g_S (\mu_V - V) + I_{\text{fluct}}(t) \\ \tau_S \frac{dI_{\text{fluct}}}{dt} = -I_{\text{fluct}} + Q_I \left(\sum_k \delta(t_e^k - t) - \sum_k \delta(t_i^k - t) \right) \end{cases} \quad (17)$$

The three variables $(\mu_V, \sigma_V, \tau_V^N)$ are achieved through the five variables of the input $(I_{\mu_V}, g_S, \nu_{in}, \tau_S, Q_I)$. We have two additional degrees of freedom, so 1) to force the input to remain in the *fluctuation-driven* regime (many events of low amplitude) we arbitrarily set the presynaptic frequency to $\nu_{in} = 2\text{kHz}$ and 2) we fixed the current time constant to: $\tau_S/\tau_m^0 = 15\%$ (i.e. $\tau_S = 4.5\text{ms}$ for $\tau_m^0 = 30\text{ms}$).

Thus, when we want to study the firing rate response as a function of $(\mu_V, \sigma_V, \tau_V^N)$, with the membrane parameters (g_L, τ_m^0, E_L) , we send an input of the form Equation 17, where $(I_{\mu_V}, g_S, \tau_S, Q_I, \nu_{in})$ follow:

$$\begin{cases} \tau_S = 0.15 \tau_m^0 \\ \nu_{in} = 2.10^3 \\ I_{\mu_V} = g_L (\mu_V - E_L) \\ g_S = g_L \left((\tau_V^N - \frac{\tau_S}{\tau_m^0})^{-1} - 1 \right) \\ Q_I = \frac{(g_L + g_S) \sigma_V \sqrt{\tau_m^0} \sqrt{\tau_V^N}}{\tau_S \sqrt{\nu_{in}}} \end{cases} \quad (18)$$

VI.8 Monitoring the stability of the cellular properties

Because the stimulation depends on the membrane properties (see the previous section VI.7), it was crucial to insure the stability of those properties during the experiments. We therefore monitored the cellular properties in time in an analogous manner to ?.

In between the episodes, we use the resting period to measure the resting membrane potential E_L and we inject a short current pulse to calculate the membrane resistance. Those quantity over time are then smoothed over a sliding window of 20 points to remove the error introduced by the evaluation over a rather short time window (Figure 4E).

The data kept in the dataset had to keep variations within $\pm 3\text{ mV}$ for E_L and below 10 % for R_m .

In addition, we quantified and monitored the stability of the firing rate response. Here, the fitted response was found to be very useful (see Results IV.2). When we fit, we do not discriminate between the early and the late measurements, the fitted function \mathcal{F} therefore provides a mean of the response across the measurement. Then we can detect variations around this mean behavior by computing the coefficient of variation of the response:

$$CV_{\nu}(\vec{x}, t_i) = \frac{\nu_{\text{out}}(\vec{x}, t_i) - \mathcal{F}(\vec{x})}{\sqrt{\mathcal{F}(\vec{x})/T_i}} \quad (19)$$

where \vec{x} represents a combination of the input $(\mu_V, \sigma_V, \tau_V^N)$, t_i the time of the measurement and T_i the duration of the measurement. Because of the intrinsic irregularity of the spiking process, we expect strong fluctuations within this curve (see Figure 4D), but the smoothen version of this curve allow to detect changes on a long time scale. For example, a strong *run-down* would correspond to a strongly decreasing CV_{ν} curve. The criteria to insure stability was to remain close enough from

a stationary Poisson process, i.e. the smoothen curve should not cross ± 1 .

Given those criteria, we expect that the effect of the remaining variability in the properties would be canceled by the randomization of the scanned input points and the use of multiple seeds.

VI.9 Theoretical models of neurons

The general model considered in this study is the inactivating Adaptative Exponential and Fire model. It is constructed by combining the theoretical models proposed in [Brette and Gerstner \(2005\)](#) and [Platkiewicz and Brette \(2011\)](#).

$$\begin{cases} C_m \frac{dV}{dt} = g_L (E_L - V) + I_{syn}(V, t) + k_a e^{\frac{V - V_{thre}}{k_a}} - I_w \\ \tau_w \frac{dI_w}{dt} = -I_w + \sum_{t_s \in \{t_{spike}\}} b \delta(t - t_s) \\ \tau_i \frac{d\theta}{dt} = -\theta + a_i (V - V_i) \mathcal{H}(V - V_i) \end{cases}$$

where $I_{syn}(V, t)$ is the current emulating synaptic activity that will create the fluctuations, I_w reproduces the I_m current ([McCormick et al., 1985](#)) and $\theta(t)$ is a variable threshold whose temporal dynamics and voltage dependence accounts for the fast decrease in sodium channel availability at depolarized levels (?).

The temporal dynamics of sodium inactivation and spike frequency adaptation were fixed to $\tau_i=5\text{ms}$ and $\tau_w = 500\text{ms}$ respectively. Also the threshold of the inactivation curve was fixed relative to the sodium activation threshold as $V_i = V_{thre} - 8\text{mV}$. The leak potential was set to $E_L=-70\text{mV}$ all along the study. All other parameters are varied along the study (see figure legends).

Finally, because of the variability of membrane time constants in the experimental data (indeed, the data show variations not only in input resistance, also in τ_m^0), the comparison for the firing response between data and theoretical models requires a careful treatment. Because when the synaptic bombardment raises, the ratio of input conductance with respect to the leak conductance μ_G/g_L raises, we scanned a fixed range in terms of $\tau_V^N=\tau_V/\tau_m^0$ (see previous section [VI.7](#)). But this means that for a given range of $\tau_V^N=\tau_V/\tau_m^0$, there will be different range of τ_V when there is a change in membrane time constant τ_m^0 , and consequently a different range of output frequency. The solution that we adopted for a relevant comparison between data and theoretical models is to simulate the models with different membrane time constants τ_m^0 reproducing the variability in experimental data. Only in Figure 2, a single model was numerically simulated with the parameters ($g_L = 2.5\text{nS}$, $C_m = 80\text{pF}$ to get $\tau_m^0=32\text{ms}$ as the average of the intracellular data). For all other figures (Figures 3, 6 and 7), where the sensitivities are presented, we simulated three models, all with the same leak conductance $g_L = 2.5\text{nS}$, but with varying capacitance to reach $\tau_m^0 \in [20, 32, 44]\text{ ms}$ to reproduce the standard deviation of the data (see previous section [VI.2](#)). The presented sensitivities were then the average of the sensitivities of the three models. Note that, even if the scaling of the firing response with the resting membrane time constant is clear in theoretical model ($\nu_{out} \propto 1/\tau_m^0$ for a given τ_V^N space), this effect was not significantly visible in the data (Pearson correlations between mean excitability and membrane time constants, $p>0.1$) presumably masked by the heterogeneity discussed in this paper.

VI.10 Starting from a simple approximation for the firing rate

The starting approximation that we will use has been introduced in ([Amit and Brunel, 1997](#)). Our situation is different, we have a more complex synaptic input but we only want the stationary firing rate, so we justify this estimate in a more abstract manner.

If a neuron has membrane potential fluctuations described by a mean μ_V , a variance σ_V and a typical autocorrelation time τ_V , then we can divide a time axis of length T (with $T \gg \tau_V$) into N bins of length τ_V . Within each of this bin, we consider that a reorganization of the membrane potential values occurs, then the bins can be considered independently, and in each, we sample randomly from the Gaussian distribution defined by μ_V and σ_V . We remain in the low firing regime ($\nu_{out} \leq 30\text{ Hz}$), so that we can neglect the repolarization dynamics and saturation effects. Then, if a spike occurs when the membrane potential crosses a threshold V_{thre}^{eff} , the probability to have a spike within a bin is the probability to be above this threshold $\Pr(V > V_{thre}^{\text{eff}})$. The number of spikes during the time $T = N\tau_V$ is $k = N \cdot \Pr(V > V_{thre}^{\text{eff}})$. The definition of the stationary firing rate is $\nu_{out} = k/T$, so that we get:

$$\nu_{out} = \frac{\Pr(V \geq V_{thre}^{\text{eff}})}{\tau_V} \quad (21)$$

i.e. in the case of a Gaussian distribution for the membrane potential:

$$\nu_{out} = \frac{1}{2\tau_V} \cdot \text{Erfc}\left(\frac{V_{thre}^{\text{eff}} - \mu_V}{\sqrt{2}\sigma_V}\right) \quad (22)$$

where the subthreshold variables μ_V , σ_V and τ_V can be calculated as a response to the synaptic input as detailed in the previous section [VI.7](#).

We will use its derivative. For a variable x being either μ_V , σ_V or τ_V^N , we get:

$$\begin{aligned} \frac{\partial \nu_{out}}{\partial x} = & -\frac{\partial \tau_V}{\partial x} \frac{\nu_{out}}{\tau_m^0} \frac{1}{\tau_V^N} + \\ & \frac{e^{-(\frac{V_{thre}^{\text{eff}} - \mu_V}{\sqrt{2}\sigma_V})^2}}{\sqrt{2\pi}\tau_m^0\tau_V^N} \cdot \left(\frac{1}{\sigma_V} \left(\frac{\partial V_{thre}^{\text{eff}}}{\partial x} - \frac{\partial \mu_V}{\partial x} \right) - \frac{\partial \sigma_V}{\partial x} \frac{V_{thre}^{\text{eff}} - \mu_V}{\sigma_V^2} \right) \end{aligned} \quad (23)$$

where V_{thre}^{eff} depends linearly on the fluctuations variables (Equation 2).

VI.11 Fitting

To render the fitting the phenomenological threshold easier, we insured that the linear coefficients of Equation 2 take similar values by normalizing the $(\mu_V, \sigma_V, \tau_V^N)$ space. The normalization factors $\mu_V^0 = -60\text{mV}$, $\delta\mu_V^0 = 10\text{mV}$, $\sigma_V^0 = 4\text{mV}$, $\delta\sigma_V^0 = 6\text{mV}$, $\tau_V^{N0} = 0.5$, $\delta\tau_V^{N0} = 1$. arbitrarily delimits the *fluctuation-driven* regime (a mean value x and an extent δx , $\forall x \in \{\mu_V, \sigma_V, \tau_V^N\}$). It is kept constant all along the study.

The fitting consisted first in a linear regression in the phenomenological threshold space of Equation 2, followed by a non-linear optimization of Equation 1 on the firing rate response. Both fitting were performed with the `leastsq` method in the `optimize` package of SciPy.

Note that the reason for not restricting the fitting to the linear regression is that you can not include the $\nu_{out} = 0$ points (because Erfc^{-1} has a singularity). Given the limited number of experimental points, such a truncation would have introduced a strong bias toward high firing response (not shown), this

motivated the introduction of the second non-linear fitting step.

VI.12 Numerical tools

All numerical simulations of single cell dynamics have been performed with custom code written in the numerical library of `python`: `numpy` and optimized with the `numba` library. For the neuronal model, each point (a mean output frequency and its standard deviation across trials) corresponds to numerical simulations running with a time step $dt=0.01\text{ms}$, for a duration of 10s and repeated 4 times with different seeds (one simulation duration: $\sim 2\text{s}$ of real time on a Dell Optiplex 9020 desktop computer). Experimental protocols and online-analysis have been written in `Elphy2`. Plots and data analysis have been done thanks to the `SciPy` package.

VII References

- Amit DJ, Brunel N (1997) Model of global spontaneous activity and local structured activity during delay periods in the cerebral cortex. *Cerebral Cortex* 7:237–252.
- Badel L, Lefort S, Berger TK, Petersen CCH, Gerstner W, Richardson MJE (2008) Extracting non-linear integrate-and-fire models from experimental data using dynamic I-V curves. *Biological Cybernetics* 99:361–370.
- Brette R, Gerstner W (2005) Adaptive exponential integrate-and-fire model as an effective description of neuronal activity. *Journal of neurophysiology* pp. 3637–3642.
- Brunel N, Sergi S (1998) Firing frequency of leaky integrate-and-fire neurons with synaptic current dynamics. *Journal of theoretical biology* 195:87–95.
- Debanne D, Campanac E, Bialowas A, Carlier E, Alcaraz G (2011) Axon physiology. *Physiological reviews* 91:555–602.
- Destexhe A, Contreras D (2006) Neuronal computations with stochastic network states. *Science* 989:85–90.
- Destexhe A, Rudolph M, Paré D (2003) The high-conductance state of neocortical neurons in vivo. *Nature Reviews Neuroscience* 4:739–751.
- Fourcaud N, Hansel D, van Vreeswijk C, Brunel N (2003) How spike generation mechanisms determine the neuronal response to fluctuating inputs. *The Journal of neuroscience* 23:11628–11640.
- Giugliano M, La Camera G, Fusi S, Senn W (2008) The response of cortical neurons to in vivo-like input current: theory and experiment: II. Time-varying and spatially distributed inputs. *Biological cybernetics* 99:303–18.
- Ilin V, Malyshev A, Wolf F, Volgshev M (2013) Fast computations in cortical ensembles require rapid initiation of action potentials. *The Journal of neuroscience : the official journal of the Society for Neuroscience* 33:2281–92.
- Kuhn A, Aertsen A, Rotter S (2004) Neuronal integration of synaptic input in the fluctuation-driven regime. *The Journal of neuroscience : the official journal of the Society for Neuroscience* 24:2345–56.
- Kyrozis A, Reichling DB (1995) Perforated-patch recording with gramicidin avoids artifactual changes in intracellular chloride concentration. *Journal of Neuroscience Methods* 57:27–35.
- La Camera G, Giugliano M, Senn W, Fusi S (2008) The response of cortical neurons to in vivo-like input current: theory and experiment : I. Noisy inputs with stationary statistics. *Biological cybernetics* 99:279–301.
- Lippiat J (2009) Whole-cell recording using the perforated patch clamp technique In Lippiat J, editor, *Potassium Channels*, Vol. 491 of *Methods in Molecular Biology*, pp. 141–149. Humana Press.
- McCormick DA, Connors BW, Lighthall JW, Prince Da (1985) Comparative electrophysiology of pyramidal and sparsely spiny stellate neurons of the neocortex. *Journal of neurophysiology* 54:782–806.
- Platkiewicz J, Brette R (2010) A threshold equation for action potential initiation. *PLoS computational biology* 6:e1000850.
- Platkiewicz J, Brette R (2011) Impact of fast sodium channel inactivation on spike threshold dynamics and synaptic integration. *PLoS computational biology* 7:e1001129.
- Rae J, Cooper K, Gates P, Watsky M (1991) Low access resistance perforated patch recordings using amphotericin B. *Journal of Neuroscience Methods* 37:15–26.
- Rauch A, La Camera G, Lüscher HR, Senn W, Fusi S, Lüscher HR (2003) Neocortical Pyramidal Cells Respond as Integrate-and-Fire Neurons to In Vivo-Like Input Currents. *J Neurophysiol* 90:1598–1612.
- Tuckwell HC, Wan FYM, Rospars JP (2002) A spatial stochastic neuronal model with Ornstein–Uhlenbeck input current. *Biological cybernetics* 86:137–145.
- Wendt DJ, Starmer CF, Grant AO (1992) Na channel kinetics remain stable during perforated-patch recordings. *The American journal of physiology* 263:C1234–C1240.